PHILOSOPHICAL TRANSACTIONS OF THE ROYAL SOCIETY A MATHEMATICAL, PHYSICAL & ENGINEERING SCIENCES

# The dynamics, prediction, and control of wing rock in high–performance aircraft

Brad S. Liebst

*Phil. Trans. R. Soc. Lond. A* 1998 **356**, 2257-2276
doi: 10.1098/rsta.1998.0273

THE ROYAL SOCIETY

# The dynamics, prediction, and control of wing rock in high-performance aircraft

By Brad S. Liebst

*Air Force Institute of Technology, Wright-Patterson Air Force Base, OH 45433, USA*

This study is an investigation of the nonlinear aircraft behaviour known as wing rock. An eight-state F-15 model is analysed by using bifurcation theory and root-locus techniques. The wing-rock onset point is identified, and small perturbation analysis is used to linearize the equations of motion about this point. The eigenstructure of the model is analysed and is used to identify the stability modes involved in this motion. A procedure is developed to predict wing-rock onset, and the critical stability derivatives involved in this behaviour are identified. The developed procedure is applied to existing F-15 data. The results show that wing rock is an unstable Dutch-roll motion and the developed wing-rock prediction parameter is accurate to within 1° of onset angle of attack (AOA).

Various simple feedback control schemes are evaluated to determine how to delay the onset of wing rock. The most effective control scheme is found to be a combination of roll rate and sideslip fixed gain feedback to the ailerons yielding a 6° improvement in the onset AOA of wing rock.

**Keywords: wing rock; aircraft dynamics; aircraft controls; nonlinear dynamics; flight mechanics; aircraft stability and control**

## 1. Introduction

Many modern-day combat aircraft exhibit lightly damped or constant-amplitude rolling oscillations at moderate to high angle of attack (AOA). These motions are commonly referred to as wing rock. Wing rock can have a wide-ranging effect on an aircraft's ability to complete its mission. Wing rock may present itself as a minor nuisance during noncritical manoeuvring, or as a major headache while trying to track an enemy target. For some configurations, wing rock is an early warning of impending departure or spin entry (Nguyen *et al*. 1980). In some aircraft, the severity of wing rock could create sufficient inertial and kinematic coupling to cause AOA excursions leading to loss of control. This problem may present itself during the landing phase as well as during manoeuvring flight.

Two different types of wing rock have been identified by previous research (Nguyen *et al*. 1980). The first is characterized by unsteady lateral motions at moderate to high AOA. These motions exhibit small-amplitude intermittent roll oscillations and may be a function of pilot–vehicle interaction. Here the roll motion is not periodic. This type of wing rock is normally associated with low-airspeed, high-AOA flight in gusty conditions such as during approach and landing. The second type of wing rock is manifested as an initially diverging oscillation which becomes periodic in nature and is generated by a limit-cycle mechanism. This motion is characterized by very

large changes in roll angle. The second form of wing rock is normally associated with high-AOA manoeuvring such as in close-in air combat. Flight procedures can normally be changed to avoid the first type of wing rock without greatly affecting mission accomplishment, but the same cannot be said about type two. If a combat aircraft is not able to track a target due to wing rock, it becomes obvious that mission accomplishment has been degraded significantly. This study deals with the second type of wing rock.

The mechanisms which cause wing rock are not fully understood. It appears that wing rock is triggered by some type of flow asymmetry, causing initial negative roll damping, and then sustained by some type of nonlinear aerodynamic roll damping (Hsu & Lan 1985). Therefore, aerodynamically, wing rock may be caused by flow separation at low speeds or shock-induced separations at transonic speeds, oscillatory aerodynamic loads produced by aircraft motion, or vortex flow dynamics over the wing and fuselage (Planeaux & Barth 1988). From the stability point of view it is postulated that wing rock is associated with a sign change in $C_{n\beta}$, reduced and nonlinear roll damping, or instability of one or more of the aircraft's longitudinal and/or lateral control modes.

Previous studies have already developed several parameters which provide indications of aircraft behaviour at high AOA. Notable are the lateral control divergence parameter (LCDP) and $C_{n\beta,\mathrm{dynamic}}$, or some combination of the two (Nguyen *et al.* 1980). These parameters have been used to predict aircraft departure sensitivity and general departure characteristics. These parameters provide general estimates of aircraft behaviour at high AOA, they are not able to specifically predict aircraft motion at high AOA. Both of these parameters were developed for MIL-F-8785C and have been carried forward in MIL-STD-1797A.

This study takes another step forward and develops a parameter that specifically predicts the onset of wing rock. Using this parameter, a procedure is developed which allows an aircraft designer, given certain stability derivatives and inertia characteristics, to predict the onset of wing rock in his design without using complicated software and costly computer time. This study also attempts to identify the relative importance of the various stability derivatives which contribute to wing rock.

Finally, various simple feedback-control schemes are evaluated to determine how to delay the onset of wing rock. Liebst & DeWitt (1997) and others (Davison 1992; Araujo & Singh 1997; Littleboy & Smith 1997) have examined the control of wing rock previously with various degrees of success. The controllers developed by Araujo & Singh (1997) and Littleboy & Smith (1997) were the following: complicated model reference adaptive and dynamic inversion. In the present research, significant improvements are demonstrated by using a simple fixed-gain combined roll rate and sideslip feedback to the ailerons.

## 2. Aircraft descriptions and equations of motion

In this section, the aircraft used is presented and the model equations of motion are developed.

The nonlinear equations of motion used in this study are linearized by using small-disturbance theory. These equations are linearized about the point at which wing rock begins during an elevator sweep. The resulting linear expressions are then used in conjunction with eigenvector data in an attempt to parametrize wing-rock motion.

Normally, the small-angle assumption (both the perturbations and the equilibrium angles are assumed to be small enough that the sines of these angles are approximately equal to the angles themselves and the cosines are equal to one) is also made to further simplify the perturbed equations of motion. In this study, some of the equilibrium angles are fairly large, so the small-angle assumption will not be made and the sines and cosines will take on their actual values.

Since wing rock is highly nonlinear, we need an efficient analysis strategy to study its behaviour. A number of previous studies have demonstrated that bifurcation analysis can be used to predict and characterize many nonlinear high-AOA behaviours of fighter aircraft (Barth 1987; Beck 1989; Carroll & Mehra 1982; Planeaux & Barth 1988; Zagaynov & Goman 1984). This study uses bifurcation theory as the first step in determining aircraft eigenstructure at the onset of wing rock. The reader is referred to Seydel (1988) for more information on bifurcation theory.

There are several software packages available to accomplish the required bifurcation calculations. This study employed AUTO, a FORTRAN package written by Doedel & Kervenez (1984). AUTO was selected because it provided the greatest flexibility and required the least modification to fulfil the needs of the present study.

Starting from a known equilibrium point, AUTO first generates the equilibrium branch containing this point. It then computes the points along the equilibrium branch by a process known as *path following*. This process works by repeatedly using known solution points to calculate nearby solutions and thereby trace out the equilibrium branch. As the path following is performed, the software detects and locates limit points, Hopf bifurcations and other bifurcation points. The program then stores information required to allow continuation of new branches that grow from these bifurcation points. AUTO is capable of returning to each of these points and performing path following along the corresponding solution branches. Resulting equilibrium branch output includes values of all states and parameters.

AUTO also possesses the ability to perform path following along periodic branches, and can thus provide limit-cycle data and some measure of the amplitude and period of the oscillatory motion.

For the present study, an eigenvector solver was added to AUTO to determine modal information along the solution branches. The eigenvector software was taken from *Matrix eigensystem routines* (Smith 1974), and adapted to meet the needs of this study.

This study uses the F-15 Eagle aircraft to validate its findings. A description of this aircraft is given in Nolan (1992). The equations of motion used in this study are nonlinear. These nonlinear relationships are based on the following assumptions.

1. The aircraft is a rigid body.
2. The aircraft has constant mass and mass properties.
3. The $x$–$z$ plane is a plane of symmetry.
4. The Earth provides a fixed reference frame in space.
5. The true velocity, $V_{\mathrm{tr}}$, AOA, $\alpha$, and sideslip angle, $\beta$, are defined as shown in figure 1.

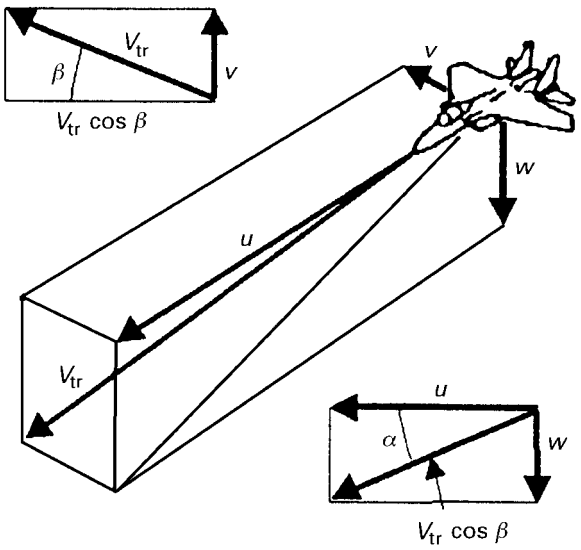


Figure 1. Aircraft velocity components.

Based on the above assumptions, the six-degrees-of-freedom (DOF) equations of motion are given in terms of non-dimensional aerodynamic force and moment coefficients (McRuer *et al.* 1973)

$$\dot{\alpha} = q - \left[\frac{QS}{mV_{tr}}C_x - \frac{g}{V_{tr}}\sin\theta + r\sin\beta\right]\sin\alpha\sec\beta + \left[\frac{QS}{mV_{tr}}C_z + \frac{g}{V_{tr}}\cos\theta\cos\phi - p\sin\beta\right]\cos\alpha\sec\beta, \tag{2.1}$$

$$\dot{\beta} = -\left[\left(\frac{QS}{mV_{tr}}C_x - \frac{g}{V_{tr}}\sin\theta\right)\sin\beta + r\right]\cos\alpha + \left[\frac{QS}{mV_{tr}}C_y + \frac{g}{V_{tr}}\cos\theta\sin\phi\right]\cos\beta - \left[\left(\frac{QS}{mV_{tr}}C_z - \frac{g}{V_{tr}}\cos\theta\cos\phi\right)\sin\beta - p\right]\sin\alpha, \tag{2.2}$$

$$\dot{V}_{tr} = V_{tr}\left[\frac{QS}{mV_{tr}}C_x - \frac{g}{V_{tr}}\sin\theta\right]\cos\alpha\cos\beta + V_{tr}\left[\frac{QS}{mV_{tr}}C_y + \frac{g}{V_{tr}}\cos\theta\sin\phi\right]\sin\beta + V_{tr}\left[\frac{QS}{mV_{tr}}C_z + \frac{g}{V_{tr}}\cos\theta\cos\phi\right]\sin\alpha\cos\beta, \tag{2.3}$$

$$\dot{p} = \left[-\left[\frac{I_z - I_y}{I_x} + \frac{I_{xz}^2}{I_xI_z}\right]qr + \left[1 - \frac{I_y - I_x}{I_z}\right]\frac{I_{xz}}{I_x}pq + \frac{QSb}{I_x}\left[C_1 + \frac{I_{xz}}{I_z}C_n\right]\right]\left[1 - \frac{I_{xz}^2}{I_xI_z}\right]^{-1}, \tag{2.4}$$

$$\dot{q} = \frac{QSc}{I_y} C_m + \frac{I_z - I_x}{I_y} pr + \frac{I_{xz}}{I_y}(r^2 - p^2), \tag{2.5}$$

$$\dot{r} = \left[\left[\frac{I_{xz}^2}{I_x I_z} - \frac{I_y - I_x}{I_z}\right] pq - \left[1 + \frac{I_z - I_y}{I_x}\right]\frac{I_{xz}}{I_z} qr + \frac{QSb}{I_z}\left[\frac{I_{xz}}{I_x} C_1 + C_n\right]\right]\left[1 - \frac{I_{xz}^2}{I_x I_z}\right]^{-1}, \tag{2.6}$$

$$\dot{\phi} = p + q \tan\theta \sin\phi + r \tan\theta \cos\phi, \tag{2.7}$$

$$\dot{\theta} = q \cos\theta - r \sin\theta. \tag{2.8}$$

The expansions of the aerodynamic force and moment coefficients were extracted from a McDonnell Aircraft Company F-15 simulator program (McDonnell Aircraft Company 1976, 1981). The coefficients were obtained from simulator data (combined wind-tunnel and flight-test data) tabulated for Mach numbers from 0.3–2.5 and from 0–80 000 feet. Mach number and altitude dependence had been eliminated by selecting data at 0.6 Mach and 20 000 feet. The data were curve-fitted to multivariable polynomials to provide a more efficient computer model. The equations are as follows:

$$C_x = C_L(\alpha, \delta e)\sin\alpha - C_D(\alpha, \delta e)\cos\alpha + \frac{T}{(QS)}, \tag{2.9}$$

$$C_y = C_{y_\beta}(\alpha, |\beta|, \delta e)\beta + C_{y_{\delta a}}(\alpha)\delta a + C_{y_{\delta r}}(\alpha, |\delta r|)\delta r + \left[\frac{b}{2V_{\mathrm{tr}}}\right][C_{y_r}(\alpha) r + C_{y_p}(\alpha) p], \tag{2.10}$$

$$C_z = -C_L(\alpha, \delta e)\cos\alpha - C_D(\alpha, \delta e)\sin\alpha, \tag{2.11}$$

$$C_l = C_{l_\beta}(\alpha, |\beta|)\beta + C_{l_{\delta a}}(\alpha, \delta e)\delta a + C_{l_{\delta r}}(\alpha, |\delta r|)\delta r + \left[\frac{b}{2V_{\mathrm{tr}}}\right][C_{l_r}(\alpha) r + C_{l_p}(\alpha) p], \tag{2.12}$$

$$C_m = C_{m_\alpha}(\alpha, \delta e)\alpha - \left[\frac{c}{2V_{\mathrm{tr}}}\right] C_{m_q}(\alpha) q + \frac{T\delta t}{(Qsc)}, \tag{2.13}$$

$$C_n = C_{n_\beta}(\alpha, |\beta|, \delta e)\beta + C_{n_{\delta a}}(\alpha)\delta a + C_{n_{\delta r}}(\alpha, |\beta|, |\delta r|, \delta e)\delta r + \left[\frac{b}{2V_{\mathrm{tr}}}\right][C_{n_p}(\alpha) p + C_{n_r}(\alpha) r]. \tag{2.14}$$

Each of the aerodynamic coefficients and stability derivatives in the above equations are functions of the aircraft states and the control-surface deflections shown. For a more detailed description of the aerodynamic-coefficient development, see Barth (1987). With these coefficients, the eight-state F-15 model is fully developed.

A single solution to the equilibrium system is required to begin the bifurcation continuation process. Straight, wings-level flight was chosen as a starting point because equilibrium solutions to the equations of motion can be found easily. Based on these assumptions, most of the states are zero. By then simplifying the system and spec-

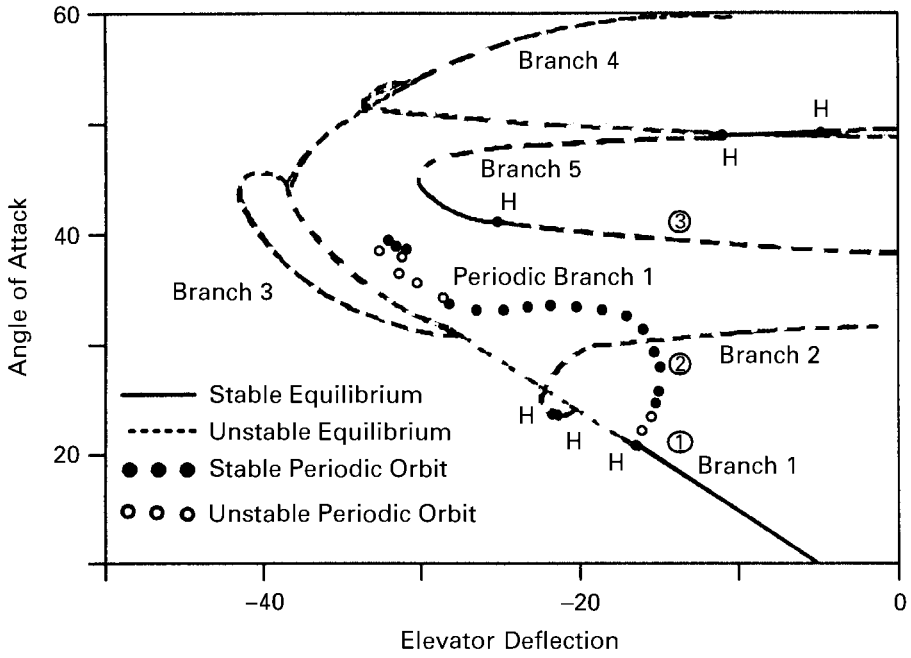


Figure 2. $\alpha$ bifurcation diagram for the F-15.

ifying one of the remaining states, the system can be solved simultaneously. The specified parameter chosen was AOA and its initial value was 10°.

## 3. Bifurcation analysis

The bifurcation parameter chosen for the bifurcation study was the F-15 stabilator deflection. Angle of attack was increased in small steps as stabilator deflection was increased (in the negative direction) from the starting point. This results in a straight pull-up manoeuvre being *flown* by the model. The point at which wing rock begins will be referred to as the *trigger point*.

The bifurcation diagram of AOA for the stabilator sweep is shown in figure 2. Branch 1, the branch continued from the initial starting point, has zero lateral states $(\beta, p, q, r)$ along its entire length. Branches 2–5, which all result from pitchfork bifurcations, have non-zero lateral states and each represents two branches which are symmetric with respect to the $x$–$z$ plane. The periodic branch emanating from the Hopf bifurcation on branch 1 is also shown.

If we assume that the aircraft is in equilibrium at the starting point of $\alpha = 10°$, then, as the stabilator deflection is increased (more negative) statically, the equilibrium point progresses along branch 1. This would be true assuming no disturbance, such as a wind gust, is large enough to result in a jump to another stable state along another equilibrium branch or periodic branch. As the stabilator deflection reaches the value at which the Hopf bifurcation occurs, branch 1 becomes unstable. A Hopf bifurcation occurs when a complex-conjugate pair of poles crosses the imaginary axis into the right half-plane. The unstable equilibrium is an unrealizable state since the smallest disturbance will cause the state trajectory to diverge from equilibrium. Therefore, as the stabilator deflection increases past the critical value at the Hopf

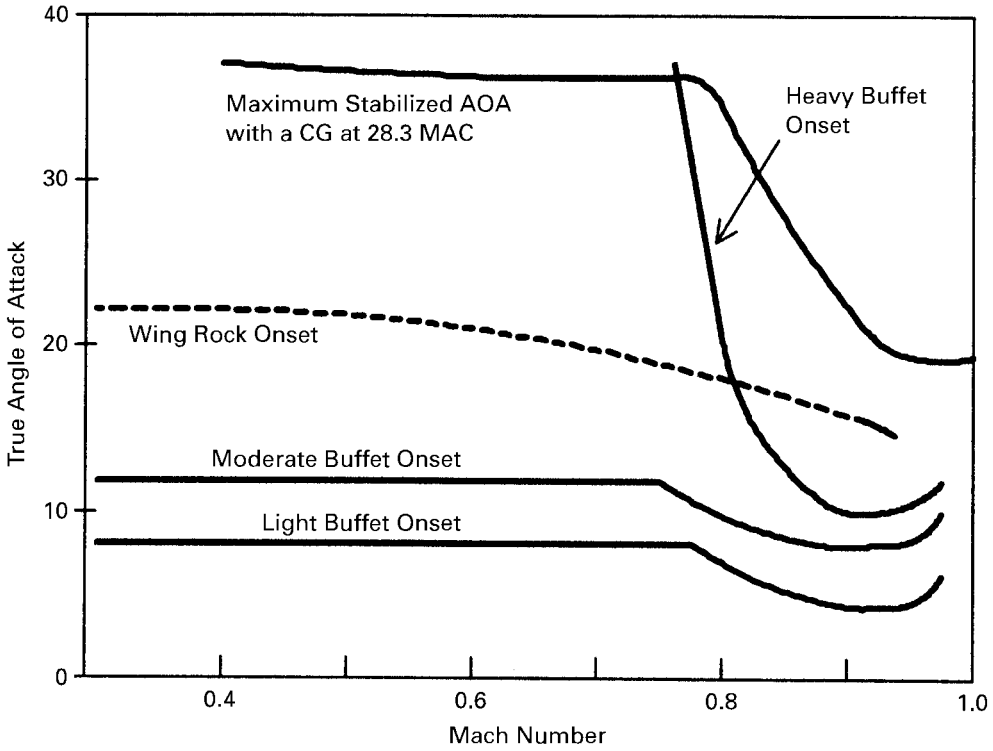


Figure 3. F-15 flight-test results.

Table 1. *State values at the Hopf point for F-15*

| $\alpha$ | $\beta$ | roll rate | pitch rate | yaw rate | $\theta$ | $\phi$ | $V_{\mathrm{tr}}$ |
|---|---|---|---|---|---|---|---|
| 21.5° | 0 | 0 | 0 | 0 | 13° | 0 | 275 feet $\mathrm{s}^{-1}$ (84 m $\mathrm{s}^{-1}$) |

bifurcation point, a jump must occur to another attractor, in this case, to the limit cycle represented by periodic branch 1 at this elevator deflection. The phenomenon which causes this jump occurs during the transition from the stable equilibrium portion of branch 1 to the stable limit-cycle portion of periodic branch 1. This jump actually represents the onset of wing rock, and the trigger point is the Hopf bifurcation point located on branch 1. This point occurs at $\alpha = 21.5°$. Wing rock begins here, and we will demonstrate later on that this coincides with the complex-conjugate pair of Dutch-roll eigenvalues migrating into the right half-plane. This point will be critical to the remainder of the analysis. The state values at this Hopf bifurcation point are presented in table 1. These findings agree reasonably well with previous F-15 flight test results (Air Force Flight Test Center 1976) for Mach equal to 0.6. These test results are shown in figure 3.

## 4. Eigenvalue analysis

The AUTO routine was modified such that the eigenvalues and eigenvectors of the state matrix at all solution points were returned in addition to the bifurcation data.

Table 2. *Eigenvalues at* $\alpha = 10.0$ *and* $21.5^\circ$ *for F-15*

| | $\alpha = 10.0^\circ$ | $\alpha = 21.5^\circ$ |
|---|---|---|
| short period mode | $-0.53 \pm 1.43$i | $-0.41 \pm 1.2$i |
| phugoid mode | $-0.003 \pm 0.109$i | $-0.040 \pm 0.15$i |
| Dutch-roll mode | $-0.28 \pm 4.3$i | $0.0 \pm 1.10$i |
| roll mode | $-0.798$ | $-0.491$ |
| spiral mode | $-0.023$ | $-0.290$ |

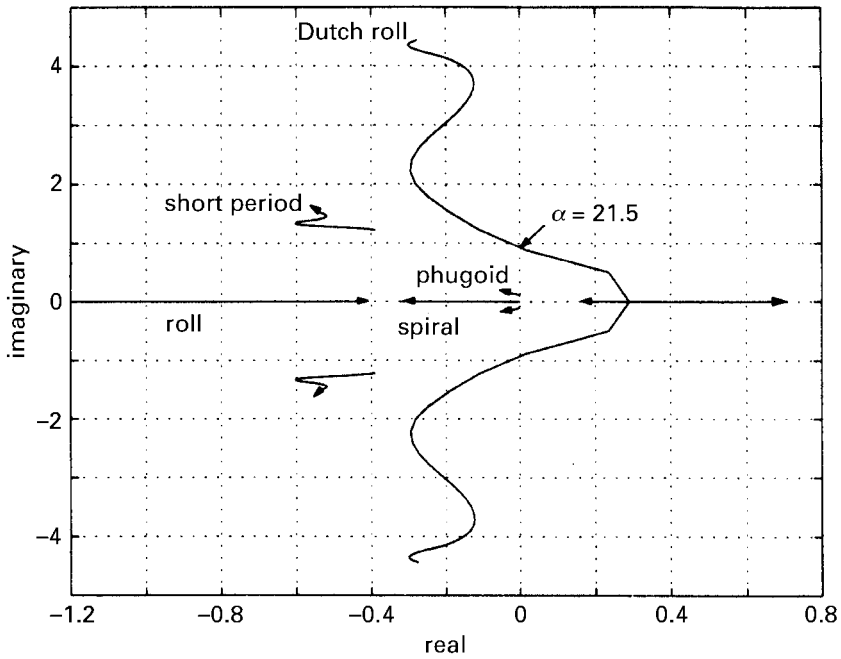


Figure 4. Root locus for the F-15 varying $\alpha$.

Thus, normal root loci with AOA can be generated. Table 2 shows the eigenvalues for $\alpha = 10.0$ and $21.5^\circ$. The F-15 displays the classic longitudinal and lateral stability modes of a conventional aircraft design.

The $21.5^\circ$ case shows the point where wing rock is triggered. As can be seen in table 2 the Dutch-roll eigenvalues are on the imaginary axis at this point and migrate into the right half-plane as $\alpha$ increases. This is easier to see in figure 4, which depicts a conventional root-locus plot for varying $\alpha$. Throughout this AOA change, the plot shows that as $\alpha$ is increased, the short-period mode initially becomes more stable then moves toward the right half-plane. The phugoid mode moves towards increased stability during the $\alpha$ increase. From figure 4 it is concluded that the longitudinal modes have little, if any, effect on the wing-rock behaviour. As can be seen, the roll mode moves toward the origin and the spiral mode moves further into the left half-plane and continues toward increasing stability. The roll mode does not cross into the right half-plane over the AOA range depicted. The Dutch-roll mode on the other hand, moves toward the right half-plane as $\alpha$ is increased. The motion is

neutrally stable at $\alpha = 21.5°$ and becomes unstable shortly thereafter. The point of neutral stability coincides with the Hopf bifurcation point on branch 1 (figure 2). The Dutch-roll mode continues further into the right half-plane as $\alpha$ is increased and eventually moves to the positive real axis. From the root loci, it appears that wing rock is an unstable Dutch-roll motion as predicted by several authors (Nguyen *et al*. 1980; Nguyen & Ross 1988; Ross 1978). At low AOA, Dutch-roll is normally approximated by a flat motion which does not contain much roll-angle change. As $\alpha$ is increased, previous research has shown that this motion becomes predominantly a roll oscillation with little yaw change (Nguyen *et al*. 1980). Thus we would expect that the eigenvector data would show that the critical states involved in this unstable motion are $\beta$, $p$ and $\phi$.

## 5. Linearization around the trigger point

In order to derive an expression that would indicate that wing rock has been triggered, the nonlinear equations of motion have been linearized about the solution point which places the Dutch-roll eigenvalues on the imaginary axis (Hopf bifurcation point). The following are the linearized equations assuming $C_{x_0} = C_{y_0} = C_{z_0} = 0$:

$$\Delta\dot{\alpha} = \left[\frac{g}{V_0}(\sin\theta_0\cos\alpha_0 - \cos\theta_0\sin\alpha_0) + \frac{QS}{mV_0}(C_{z_\alpha}\cos\alpha_0 - C_{x_\alpha}\sin\alpha_0)\right]\Delta\alpha + \Delta q + \left(\frac{g}{V_0}\cos\theta_0\sin\alpha_0 - \frac{g}{V_0}\sin\theta_0\cos\alpha_0\right)\Delta\theta, \quad (5.1)$$

$$\Delta\dot{\beta} = \left[\frac{g}{V_0}(\sin\theta_0\cos\alpha_0 - \sin\alpha_0\cos\theta_0) + \frac{QS}{mV_0}C_{y_\beta}\right]\Delta\beta + \left[\frac{QS}{mV_0}C_{y_p} + \sin\alpha_0\right]\Delta p - \cos\alpha_0\Delta r + \frac{g}{V_0}\cos\theta_0\Delta\phi, \quad (5.2)$$

$$\Delta\dot{p} = A((C_{l_\alpha} + BC_{n_\alpha})\Delta\alpha + (C_{l_\beta} + BC_{n_\beta})\Delta\beta + (C_{l_p} + BC_{n_p})\Delta p + (C_{l_r} + BC_{n_r})\Delta r + (C_{l_v} + BC_{n_v})\Delta V), \quad (5.3)$$

$$\Delta\dot{q} = \frac{Qsc}{I_z}(C_{m_\alpha}\Delta\alpha + C_{m_q}\Delta q + C_{m_v}\Delta V), \quad (5.4)$$

$$\Delta\dot{r} = A((BC_{l_\beta} + C_{n_\beta})\Delta\beta + (BC_{l_p} + C_{n_p})\Delta p + (BC_{l_r} + C_{n_r})\Delta r + (BC_{l_v} + C_{n_v})\Delta V), \quad (5.5)$$

$$\Delta\dot{\theta} = \Delta q, \quad (5.6)$$

$$\Delta\dot{\phi} = \Delta p, \quad (5.7)$$

$$\Delta\dot{V} = \left[(g\sin\theta_0\sin\alpha_0 + g\cos\theta_0\cos\alpha_0) + \frac{QS}{mV_0}(C_{x_\alpha}\cos\alpha_0 + C_{z_\alpha}\sin\alpha_0)\right]\Delta\alpha + (-g\cos\theta_0\cos\alpha_0 - g\sin\alpha_0\sin\theta_0)\Delta\theta. \quad (5.8)$$

The three steady-state conditions of $\alpha_0$, $\theta_0$ and $V_0$ have been left as variables at this point to allow their influence to be seen in expression development. For the linearized equations (5.1)–(5.8), $A$ and $B$ are defined in equation (5.9) and will remain as such

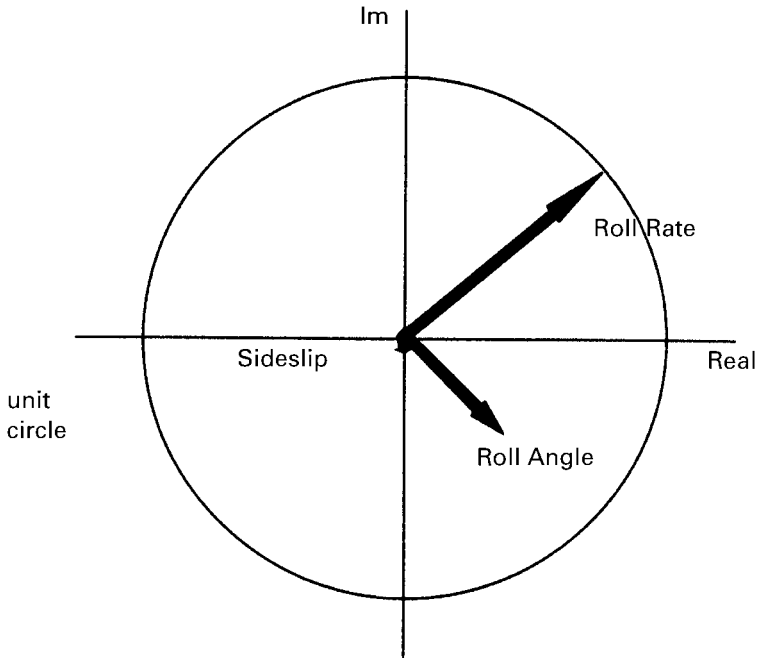


Figure 5. Magnitude of wing-rock eigenvector at the trigger point.

throughout the remainder of this document:

$$A = \frac{Qsb}{I_x} \Big/ \left[1 - \frac{I_{xz}^2}{I_x I_z}\right], \qquad B = \frac{I_{xz}}{I_x}. \tag{5.9}$$

## 6. Eigenvector analysis

For this study, the AUTO routine was modified to produce eigenvector data at each solution point. Figure 5 shows the relationship of the relative magnitudes of each of the components of the Dutch-roll eigenvector at AOA = 21.5° for the F-15. The only states that have a magnitude large enough to be seen are $p$, $\phi$ and $\beta$. The vectors show that longitudinal and lateral motion are in fact decoupled. The critical states involved in Dutch-roll behaviour are now $p$, $\phi$ and $\beta$. The magnitude of $r$ is so small that it can be disregarded. The vectors confirm previous research that Dutch-roll motion consists of a significant amount of yaw at low AOA, and as AOA is increased the motion becomes dominated by rolling motion (Nguyen *et al.* 1980). At low AOA, Dutch-roll is often approximated by a two-DOF expression eliminating the roll contribution. When wing rock is triggered at higher $\alpha$, the eigenvector structure of the system reveals that only the primary states of $\beta$, $\phi$ and $p$ need remain. Thus a lower-order approximate system will be based solely on the following equations:

$$\Delta\dot{\beta} = \left[\frac{g}{V_0}\sin(\theta_0 - \alpha_0) + \frac{QS}{mV_0}C_{y_\beta}\right]\Delta\beta + \left[\frac{QS}{mV_0}C_{y_p} + \sin\alpha_0\right]\Delta p + \frac{g}{V_0}\cos\theta_0\Delta\phi, \tag{6.1}$$

$$\Delta\dot{p} = A(C_{l_\beta} + BC_{n_\beta})\Delta\beta + A(C_{l_p} + BC_{n_p})\Delta p, \tag{6.2}$$

$$\Delta\dot{\phi} = \Delta p. \tag{6.3}$$

## 7. Characteristic equation

In order to study the triggering of wing rock, the characteristic equation of the new approximate state equations must be determined. The characteristic equation of the above approximate equations is shown below in expanded polynomial form. The spiral mode has been eliminated from this approximation:

$$\begin{aligned} s^3 - \left[\frac{g}{V_0}\sin(\theta_0-\alpha_0) + \frac{QS}{mV_0}C_{y_\beta} + A(C_{l_p} + BC_{n_p})\right]s^2 \\ + \left[A(C_{l_p} + BC_{n_p})\left[\frac{g}{V_0}\sin(\theta_0-\alpha_0) + \frac{QS}{mV_0}C_{y_\beta}\right]\right. \\ \left. - A(C_{l_\beta} + BC_{n_\beta})\left(\frac{QS}{mV_0}C_{y_p} + \sin\alpha_0\right)\right]s - \frac{g}{V_0}A(C_{l_\beta} + BC_{n_\beta})\cos\theta_0 = 0. \end{aligned} \tag{7.1}$$

The expression itself looks fairly complicated, and examining it does not immediately reveal anything. Upon examining equation (5.9) closely, equation (7.1) may be further simplified. For fighter-type aircraft, most of the mass is concentrated along the aircraft's $x$-axis. This mass distribution leads to a relatively small resistance to rotation about the $x$-axis. Three products of inertia, $I_{xy}$, $I_{yz}$ and $I_{xz}$, appear in the aircraft equations of motion for a rigid aircraft. By virtue of symmetry, $I_{xy}$ and $I_{yz}$ are both equal to zero. $I_{xz}$ on the other hand is not zero in most cases. $I_{xz}$ can be thought of as the measure of the uniformity of mass distribution about the $x$-axis. The axis about which $I_{xz}$ is equal to zero is defined as the principle inertia axis, and the mass of the aircraft can be considered to be concentrated on this axis. The inertia axis is rarely coincident with the aircraft centreline, therefore the $I_{xz}$ parameter cannot be set to zero. However, for fighter-type aircraft this term is relatively small when compared to the $I_z$ and $I_y$ terms. Therefore, the $I_{xz}/I_z$ term is small in comparison to one. The same is true of the $I_{xz}^2/I_xI_z$ term in the variable $A$. Thus $A$ may now be represented by

$$A = \frac{Qsb}{I_x}, \tag{7.2}$$

and the terms multiplied by $B$ can be disregarded due to their relative size. The polynomial is now

$$\begin{aligned} s^3 - \left[\frac{g}{V_0}\sin(\theta_0-\alpha_0) + \frac{QS}{mV_0}C_{y_\beta} + AC_{l_p}\right]s^2 + \left[AC_{l_p}\left[\frac{g}{V_0}\sin(\theta_0-\alpha_0) + \frac{QS}{mV_0}C_{y_\beta}\right]\right. \\ \left. - AC_{l_\beta}\left(\frac{QS}{mV_0}C_{y_p} + \sin\alpha_0\right)\right]s - AC_{l_\beta}\frac{g}{V_0}\cos\theta_0 = 0. \end{aligned} \tag{7.3}$$

The Dutch-roll mode lies on the imaginary axis at the trigger point. Therefore, at this point it becomes convenient to view the polynomial in the frequency domain. At the trigger point, the real portion of $s$ is zero, so $s$ can be replaced by $\mathrm{i}\omega$. Rewriting the polynomial in simpler form, the expression becomes

$$A_1s^3 - A_2s^2 + A_3s - A_4 = 0, \tag{7.4}$$

now substituting $s = \mathrm{i}\omega$

$$-A_1\mathrm{i}\omega^3 + A_2\omega^2 + A_3\mathrm{i}\omega - A_4 = 0, \tag{7.5}$$

grouping the real and imaginary parts yields

$$(+A_2\omega^2 - A_4) + (-A_1\omega^3 + A_3\omega)\mathrm{i} = 0. \tag{7.6}$$

Each portion of equation (7.6) must equal zero for the equality to hold. This results in two equalities

$$+A_2\omega^2 - A_4 = 0, \tag{7.7}$$

$$-A_1\omega^3 + A_3\omega = 0. \tag{7.8}$$

The wing-rock motion occurs at a frequency other than zero so an $\omega$ may be factored from equation (7.8) yielding

$$-A_1\omega^2 + A_3 = 0. \tag{7.9}$$

Multiplying equation (7.7) by $A_1$ and equation (7.9) by $A_2$, and subsequently adding the expressions will remove frequency dependence and produce

$$A_2A_3 - A_1A_4 = 0. \tag{7.10}$$

When equation (7.10) is satisfied, wing rock is triggered. The coefficients are

$$\left.\begin{aligned} A_1 &= 1, \\ A_2 &= \left[\frac{g}{V_0}\sin(\theta_0 - \alpha_0) + \frac{QS}{mV_0}C_{y_\beta} + AC_{l_p}\right], \\ A_3 &= AC_{l_p}\left[\frac{g}{V_0}\sin(\theta_0 - \alpha_0) + \frac{QS}{mV_0}C_{y_\beta}\right] - AC_{l_\beta}\left[\frac{QS}{mV_0}C_{y_p} + \sin\alpha_0\right], \\ A_4 &= AC_{l_\beta}\frac{g}{V_0}\cos\theta_0. \end{aligned}\right\} \tag{7.11}$$

The left-hand side of equation (7.10) will be labelled $X_\phi$. Thus when $X_\phi$ is zero, wing rock is triggered. The expanded expression for the trigger parameter $X_\phi$ is

$$\begin{aligned} X_\phi = \left[\frac{g}{V_0}\sin(\theta_0 - \alpha_0) + \frac{QS}{mV_0}C_{y_\beta} + AC_{l_p}\right] + \left[AC_{l_p}\left[\frac{g}{V_0}\sin(\theta_0 - \alpha_0) + \frac{QS}{mV_0}C_{y_\beta}\right]\right. \\ \left. - AC_{l_\beta}\left[\frac{QS}{mV_0}C_{y_p} + \sin\alpha_0\right]\right] - \left(AC_{l_\beta}\frac{g}{V_0}\cos\theta_0\right). \end{aligned} \tag{7.12}$$

## 8. Validation of expression

The goal of this study is to be able to predict wing rock without using complicated software such as the AUTO routine. Thus, the trigger point, $X_\phi$, should go to zero at the Hopf point predicted by AUTO. AUTO has provided the state values at the equilibrium points. Using this information, $X_\phi$ has been calculated over the AOA range of interest. These data are presented as the solid line in figure 6.

As can be seen in figure 6, the trigger parameter becomes zero near 22°. Here, the trigger parameter predicts wing-rock onset at an AOA of 22°. The bifurcation analysis predicted the AOA for wing-rock onset as 21.5°. Hence, for the F-15, the flight test results (Air Force Flight Test Center 1976) shown in figure 3, the bifurcation results, and the trigger parameter results all correlate well.

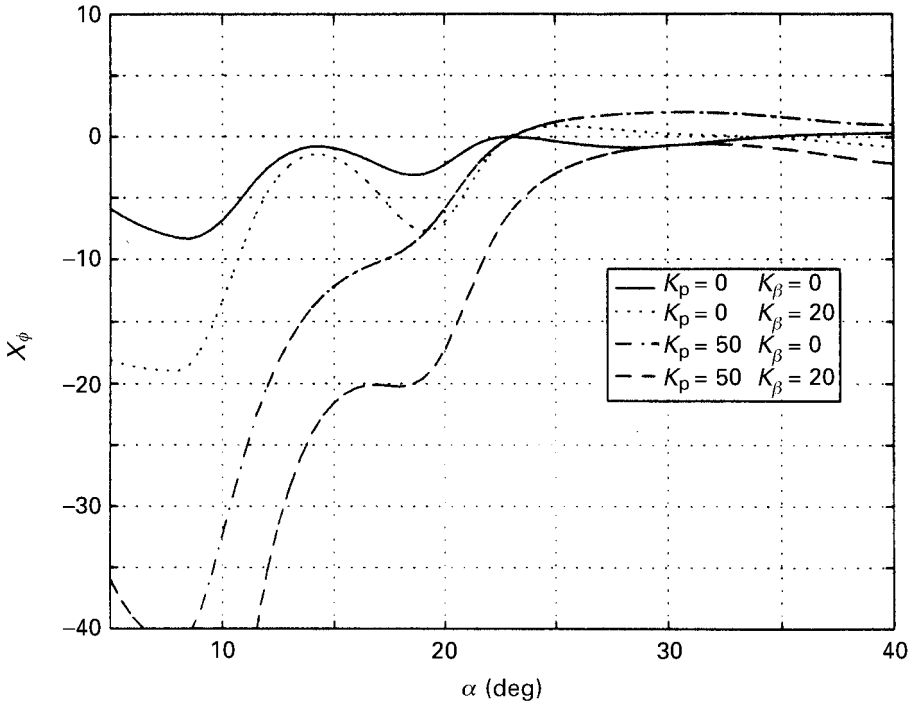


Figure 6. Trigger parameter versus AOA for the F-15.

## 9. Prediction procedure

Given the aircraft stability derivatives, inertia data and physical characteristics, we should be able to predict the AOA and airspeed at which an aircraft will wing rock by using the following iterative procedure. The following procedure is based on an aircraft operating at an equilibrium condition.

1. The first step in this process is to choose an AOA as an initial starting point. This step will provide $\alpha_0$.
2. At an equilibrium condition the moment coefficient will equal zero. Therefore, with $C_m = 0$ and $C_m(\alpha_0, \delta e_0)$ the elevator deflection can be found.
3. By combining the following equations, the initial pitch angle can be found (McRuer *et al*. 1973).

$$mg \sin\theta_0 = C_{X_0} \tfrac{1}{2}\rho V_0^2 S, \tag{9.1}$$

$$-mg \cos\theta_0 = C_{Z_0} \tfrac{1}{2}\rho V_0^2 S, \tag{9.2}$$

with

$$C_{X_0} = f(\alpha_0, \delta e_0), \tag{9.3}$$

$$C_{Z_0} = f(\alpha_0, \delta e_0), \tag{9.4}$$

yields

$$\theta_0 = \tan^{-1}(C_{X_0}/C_{Z_0}). \tag{9.5}$$

4. With the initial AOA, pitch angle and elevator deflection, equation (9.1) can be rewritten to solve for $V_0$.

$$V_0 = \left[\frac{2mg\sin\theta_0}{C_{X_0}\rho S}\right]^{1/2}. \tag{9.6}$$

5. There is now enough information to compute $X_\phi$ from equation (7.12).

6. Repeat steps 1–5 until the angle where $X_\phi$ equals zero is found. A sign change in the triggering parameter would indicate that the step size is too big and the critical angle has already been exceeded.

## 10. Critical stability derivatives

A quick inspection of equation (7.12) reveals that four stability derivatives are critical to predicting the onset of wing rock. These derivatives are: $C_{y_p}$, side force due to roll rate; $C_{y_\beta}$, side force due to sideslip; $C_{l_p}$, roll damping; and $C_{l_\beta}$, rolling moment due to sideslip.

The contribution of $C_{y_p}$ to the trigger parameter is in fact small. The sideforce coefficient due to roll-rate parameter is normally two orders of magnitude smaller that the sine of the equilibrium AOA, and for many modern configurations $C_{y_p}$ is zero (Roskam 1979). Therefore, $C_{y_p}$ has little or no effect on the actual value of the trigger parameter and its contribution can be neglected.

$C_{y_\beta}$, the sideforce due to sideslip, provides a small contribution to the $A_2$ coefficient in the trigger parameter expression. This contribution is one order of magnitude smaller than the contribution of the roll moment due to sideslip. While the derivative is large enough to be considered, its contribution does not require any significant analysis.

The findings of this study agree with the findings of Johnston *et al.* (1980). The critical stability derivatives contributing to the onset of wing rock are: $C_{l_p}$, roll damping; and $C_{l_\beta}$, roll moment due to sideslip.

$C_{l_p}$ is a function of wing sweep, aspect ratio and the wing's lift curve slope. An aircraft with a straight, highly efficient, high-aspect-ratio wing would have a large negative value of $C_{l_p}$ and hence would exhibit high roll damping. Thus, a fighter aircraft with highly swept, thin, low-aspect-ratio wings would exhibit poor roll damping. Any roll motion the aircraft exhibits will be countered by this derivative.

$C_{l_\beta}$ is often referred to as the lateral-stability or dihedral-effect derivative. This derivative describes an aircraft's ability to produce a rolling moment due to a sideslip angle. For positive lateral stability, a positive sideslip should result in a rolling moment to the left, this results in a negative $C_{l_\beta}$ for lateral stability. The number one contributor to $C_{l_\beta}$ is an aircraft's wing. Wing sweep, wing dihedral, wing position and the wing's ability to produce lift all greatly effect $C_{l_\beta}$. An increase in wing sweep, wing dihedral and $C_{L_\alpha}$ will all produce a corresponding increase in the magnitude of $C_{l_\beta}$ (Roskam 1979). The second-largest contributor to $C_{l_\beta}$ is the vertical tail, because the lift force created on the tail by a sideslip angle produces a moment about the roll axis. A conventional vertical tail has a stabilizing effect on $C_{l_\beta}$.

Previous research has shown that $C_{l_\beta}$ is directly related to Dutch-roll damping and therefore to wing-rock motion (Nguyen *et al.* 1980). Small magnitudes of $C_{l_\beta}$

result in Dutch-roll motion that is highly damped and characterized mostly by yaw and sideslip. This type of motion is characteristic of a straight-wing aircraft with negative or no dihedral angle. Fighter aircraft on the other hand, with highly swept wings, exhibit large-magnitude dihedral-effect derivatives that result in poorly damped Dutch-roll motion that consists of little yaw and sideslip and a majority of roll. Roskam (1979) has shown that a negative increase in $C_{l_\beta}$ results in a corresponding decrease in Dutch-roll damping.

From the above description of the two critical derivatives it appears that $C_{l_\beta}$ and $C_{l_p}$ are in conflict with each other and, in fact, that is the case. Both derivatives have the same response to an increase in wing efficiency (lift-curve slope). However, the most critical wing characteristics appear to be sweep, aspect ratio and dihedral angle. Thus, disregarding lift-curve slope, the characteristics that would result in a larger $C_{l_p}$ would produce a smaller $C_{l_\beta}$. This would be fine if the aircraft in question was a transport requiring a large straight-wing planform. The wing characteristics which give a fighter aircraft its increased performance also produce wing rock. A fighter aircraft with a highly swept wing designed to produce large roll rates will have a larger negative value of $C_{l_\beta}$ and a smaller negative value of $C_{l_p}$. Thus, equation (7.12) makes sense as far as this conflicting relationship between dihedral effect and roll damping is concerned. Therefore, a fighter aircraft which possesses a small negative value of $C_{l_p}$ and a relatively large value of $C_{l_\beta}$ will have a greater tendency to exhibit wing-rock characteristics. These findings agree with the open-loop critical departure parameters studied by Johnston *et al.* (1980).

We will use the fact that $C_{l_\beta}$ and $C_{l_p}$ are the most-critical stability derivatives while designing feedback controllers in the next section.

## 11. Feedback control to delay the onset of wing rock

In Liebst & DeWitt (1997), various simple fixed-gain feedback control schemes were tested on the F-15 aircraft in an attempt to delay the onset of wing rock:

1. roll rate to aileron;
2. roll rate to rudder;
3. sideslip to aileron; and
4. sideslip to rudder.

In particular, it was hoped that either roll rate to aileron (to increase effective $C_{l_p}$) or sideslip to aileron (to increase effective $C_{l_\beta}$) would prove effective. No single feedback showed a major improvement in the onset of wing rock.

We can examine the effect that roll rate to aileron feedback has upon the trigger parameter by assuming

$$\delta a = -K_p p, \tag{11.1}$$

and modifying $C_{l_p}$ with

$$(C_{l_p})_{\text{with feedback}} = (C_{l_p})_{\text{without feedback}} - K_p C_{l_{\delta a}}. \tag{11.2}$$

The graph of the new $X_\phi$ with a value of $K_p = 50$ is shown in figure 6 as the dash–dot line. We see that only a very small increase in the AOA at which $X_\phi$ crosses zero,

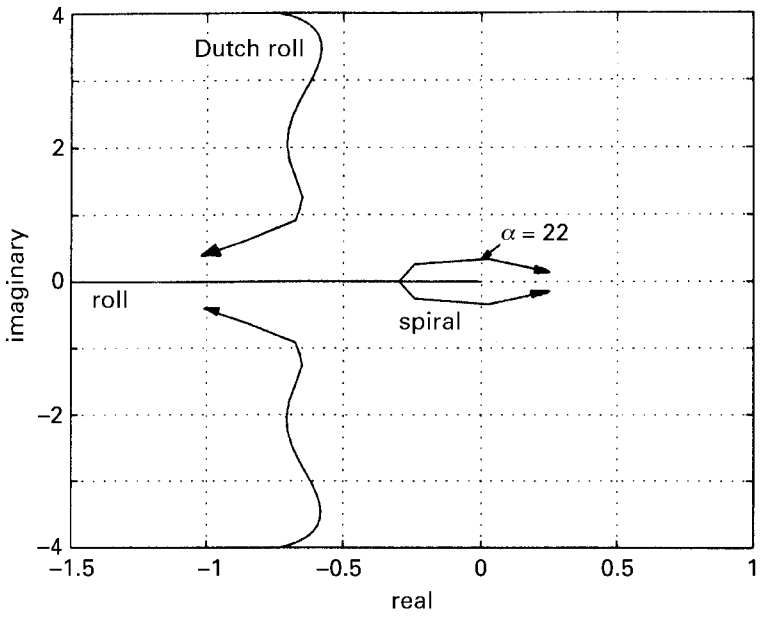


Figure 7. Root locus for the roll-rate-only feedback.

and hence only a small increase in the predicted wing-rock AOA onset. Examining figure 7 we see that the trigger parameter again accurately predicts the onset of wing rock if we compare with the actual root locus for the F-15 with feedback as given in equation (11.1). We see that roll rate to aileron feedback shows no AOA onset improvement, but the wing-rock mode is now a combined roll/spiral mode at a significantly lower wing-rock frequency than the open-loop behaviour, which recall as depicted in figure 4 was a Dutch-roll motion at a much higher frequency.

We can also examine the effect that sideslip to aileron feedback has upon the trigger parameter by assuming

$$\delta a = -K_\beta \beta, \tag{11.3}$$

and modifying $C_{l_\beta}$ with

$$(C_{l_\beta})_{\text{with feedback}} = (C_{l_\beta})_{\text{without feedback}} - K_\beta C_{l_{\delta a}}. \tag{11.4}$$

The graph of the new $X_\phi$ with a value of $K_\beta = 20$ is shown in figure 6 as the dotted line. Again, we see that only a very small increase in wing rock AOA onset is predicted. Examining figure 8, we see that the trigger parameter once again accurately predicts the onset of wing rock if we compare with the actual root locus for the F-15 with feedback as given in equation (11.3). Again there is not a major improvement in the wing-rock AOA onset.

The author next combined both the sideslip and roll rate to aileron feedbacks together. Shown as a dashed line in figure 6 is the trigger parameter plot for a system which has feedback that is the sum of equations (11.1) and (11.3) with $K_\beta = 20$ and $K_p = 50$. We see that combined $\beta$ and $p$ feedback shows no crossing of the zero line, but does come close near $\alpha = 30°$, hinting at a possible wing rock near $\alpha = 30°$. Figure 9 shows the actual root locus for the F-15 with feedback as given by the sum of equations (11.1) and (11.3). The root locus for the combined $\beta$ and $p$

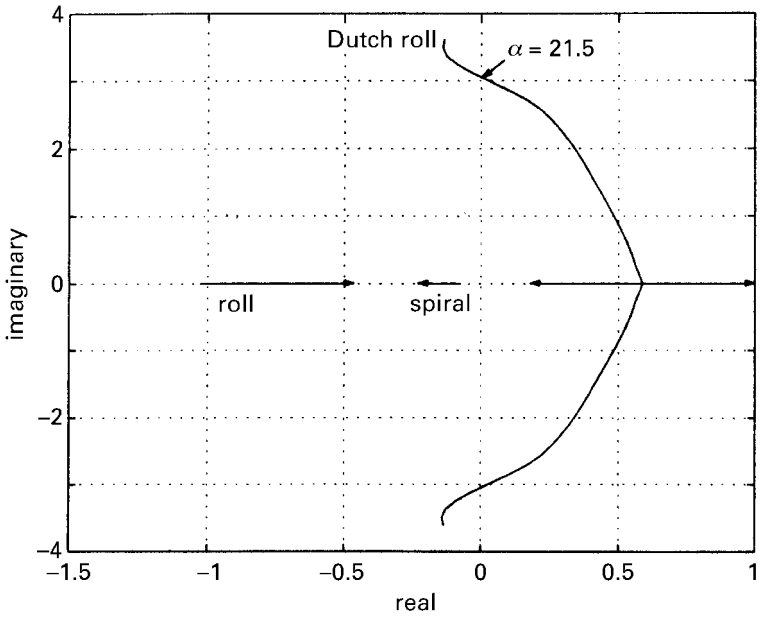


Figure 8. Root locus for the sideslip-only feedback.

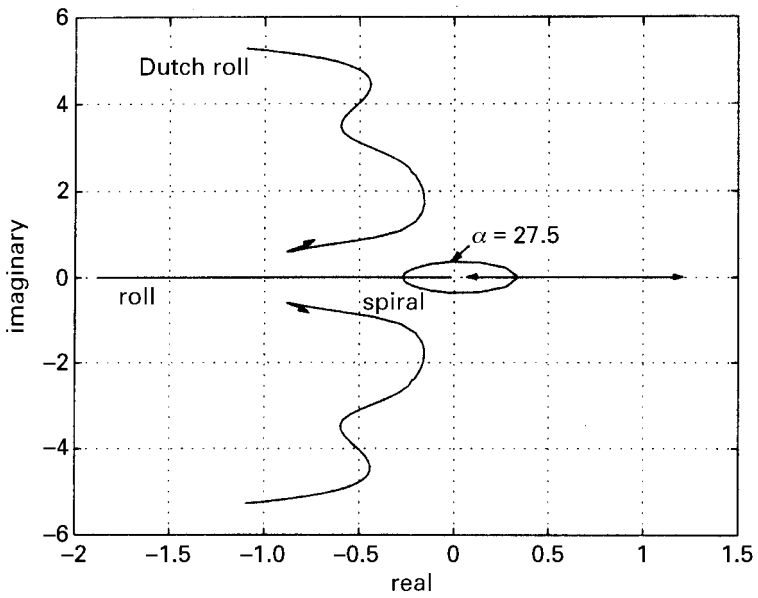


Figure 9. Root locus for the combined roll-rate and sideslip feedback.

feedback shows behaviour like that of the $p$-alone feedback, i.e. the wing-rock mode is now a combined roll/spiral mode with a significantly lower wing-rock frequency, but now with a significant 6° increase (i.e. from 21.5° to 27.5°) in AOA onset. The $X_\phi$ predicted no wing rock, but hinted at a wing rock at $\alpha \cong 30°$ which does in fact match well with the closed-loop root locus. The increase in AOA onset is certainly

noteworthy, but so is the fact that the wing-rock frequency is reduced, which makes it much easier for the pilot to correct.

Clearly, more sophisticated lead-lag networks and additional feedback channels such as $\phi$ may produce even greater improvements in AOA onset, but are not part of this limited investigation.

## 12. Conclusions

The following conclusions are based on a fighter aircraft with a swept wing manoeuvring near the 1-G stall.

1. For an unaugmented aircraft, the rolling oscillations that are commonly referred to as wing rock are actually unstable Dutch-roll motions. These oscillations usually precede the stall and for some configurations are a good indicator of impending departure. An unstable Dutch-roll motion may consist of considerable roll and yaw at low AOA, however, this motion becomes more of a pure rolling motion as $\alpha$ is increased.

2. The trigger parameter and the simple procedure developed to predict wing rock are fairly accurate for a swept-wing fighter design. Unlike LCDP or $C_{n\beta,\mathrm{dynamic}}$, which were developed to give a rough indication of unfavourable high-AOA behaviour, the trigger parameter ($X_\phi$) will predict the actual wing-rock onset AOA. The developed technique predicted wing-rock onset for the F-15 aircraft to within one degree of AOA.

3. Key stability derivatives involved in the trigger parameter are: $C_{l_p}$, roll damping; and $C_{l_\beta}$, dihedral effect. The critical situation for wing-rock development appears to be an increase in dihedral effect with a corresponding rapid decrease in roll damping as AOA is increased. These derivatives are mostly a function of the aircraft's wing. Airfoil type, wing placement, aspect ratio, sweepback and dihedral all have a large effect on the magnitude and sign of the critical-stability derivatives. The very wing characteristics which lend themselves to increased fighter performance also produce the undesirable handling quality of wing rock.

4. Neither sideslip to aileron or roll rate to aileron fixed-gain feedback alone provide significant improvement in the wing-rock AOA onset. However, a combination of both sideslip and roll rate to aileron feedback did provide a significant improvement in wing rock AOA onset.

## 13. Recommendations

Since the prediction technique described in this paper is based upon a linearization, it remains to be seen if the aerodynamic-flow regime of wing rock behaves in a linear manner as well. Further studies in this area need to be performed to determine if this linearization method will always work as it did with the F-15 example. In fact, the entire discipline of determining the aerodynamic mechanisms that cause wing rock needs further investigation.

The linearization and root-locus techniques described within this paper are well-accepted techniques often applied to stability and control analyses in the aircraft





PHILOSOPHICAL TRANSACTIONS OF THE ROYAL SOCIETY A MATHEMATICAL, PHYSICAL & ENGINEERING SCIENCES

industry, whereas the bifurcation technique, even though it has the ability to provide insight into an aircraft's dynamic characteristics, is not yet well accepted in either industry or academia. I believe that the reluctance by researchers to use the bifurcation technique is solely due to the lack of adequate software. Until suitable software is developed it is unlikely that the bifurcation technique will gain wide acceptance.

## References

Air Force Flight Test Center 1976 F-15A approach-to-stall/stall/post stall evaluation. AFFTC-TR-75-3 (January AD-B045115). Edwards AFB, CA: HQ AFFTC.

Araujo, A. & Singh, S. 1997 Variable structure adaptive control of wing rock motion of slender delta wings. In *AIAA Atmospheric Flight Mechanics Conf.*, paper no. 97-3488. Washington, DC: American Institute of Aeronautics and Astronautics.

Barth, T. J. 1987 Determination of high angle-of-attack stability of the F-15B aircraft using bifurcation analysis. MS thesis, AFIT/GAE/AA/87D-1. School of Engineering, Air Force Institute of Technology (AU), Wright-Patterson AFB, OH.

Beck, J. A. 1989 Bifurcation analysis of a model fighter aircraft with control augmentation. MS thesis, AFIT/GAE/ENY/89D-02. School of Engineering, Air Force Institute of Technology (AU), Wright-Patterson AFB, OH.

Carroll, J. V. & Mehra, R. K. 1982 Bifurcation analysis of nonlinear aircraft dynamics. *J. Guidance Control* **5**, 529–536.

Davison, M. 1992 An examination of wing rock for the F-15. MS thesis, AFIT/GAE/ ENY/92M-01. School of Engineering, Air Force Institute of Technology (AU), Wright-Patterson AFB, OH.

Doedel, E. J. & Kervenez, J. P. 1984 Software for continuation problems in ordinary differential equations with applications. Preprint. Pasadena, CA: California Institute of Technology.

Hsu, C. H. & Lan, C. E. 1985 Theory of wing rock. *J. Aircraft* **22**, 920–924.

Johnston, D., Mitchell, D. & Myers, T. 1980 Investigation of high-angle-of-attack maneuver-limiting factors. Technical Report AFWAL-TR-80-3141. Wright-Patterson AFB, OH: AFWAL.

Liebst, B. & DeWitt, B. 1997 Wing rock suppression in the F-15 aircraft. In *AIAA Atmospheric Flight Mechanics Conf.*, paper no. 97-3719. Washington, DC: American Institute of Aeronautics and Astronautics.

Littleboy, D. & Smith, P. 1997 Bifurcation analysis of a high incidence aircraft with nonlinear dynamic inversion control. In *AIAA Atmospheric Flight Mechanics Conf.*, paper no. 97-3717. Washington, DC: American Institute of Aeronautics and Astronautics.

McDonnell Aircraft Company 1976 F-15 stability derivatives, mass and inertia characteristics. Part I. Report no. MDC A4172, contract no. F33657-70-0300.

McDonnell Aircraft Company 1981 F-15 flight control system description. Design note DN-1180.01-238-458 (Rev. D).

McRuer, D., Ashkenas, I. & Graham, D. 1973 *Aircraft dynamics and automatic control*. Princeton, NJ: Princeton University Press.

Nguyen, L. T. & Ross, A. J. 1988 Some observations regarding wing rock oscillations at high angles of attack. In *AIAA Atmospheric Flight Mechanics Conf.*, paper no. 88-4371-CP. Washington, DC: American Institute of Aeronautics and Astronautics.

Nguyen, L. T., Gilbert, W. P. & Ogburn, M. E. 1980 Control-system techniques for improved departure/spin resistance for fighter aircraft. NASA Technical Paper no. 1689. Langley Research Center, Hampton, VA.

Nolan, R. C. 1992 A wing rock prediction method for a high performance fighter aircraft. MS thesis, AFIT/GAE/ENY/92J-02. School of Engineering, Air Force Institute of Technology (AU), Wright-Patterson AFB, OH.

Planeaux, J. B. & Barth, T. J. 1988 High-angle-of-attack dynamic behavior of a model high-performance fighter aircraft. In *AIAA Atmospheric Flight Mechanics Conf.*, paper no. 88-4368. Washington, DC: American Institute of Aeronautics and Astronautics.

Roskam, J. 1979 *Airplane flight dynamics and automatic flight controls*. Lawrence, KS: Roskam Aviation and Engineering Corporation.

Seydel, R. 1988 *From equilibrium to chaos: practical bifurcation and stability analysis*. New York: Elsevier.

Smith, B. T. 1974 *Matrix eigensystem routines*, 2nd edn. EISPACK Guide. New York: Springer.

Zagaynov, G. I. & Goman, M. G. 1984 Bifurcation analysis of critical aircraft flight regimes. *Int. Council Aeronautical Sci.* **84**, 217–223.





PHILOSOPHICAL TRANSACTIONS OF THE ROYAL SOCIETY A MATHEMATICAL, PHYSICAL & ENGINEERING SCIENCES